Life under a black sun

Tomáš Opatrný and Lukáš RichterekPavel Bakala

Citation: Am. J. Phys. **85**, (2017); doi: 10.1119/1.4966905
View online: http://dx.doi.org/10.1119/1.4966905
View Table of Contents: http://aapt.scitation.org/toc/ajp/85/1
Published by the American Association of Physics Teachers

Life under a black sun

Tomáš Opatrný[a] and Lukáš Richterek[b]
Faculty of Science, Palacký University, 17. Listopadu 12, 77146 Olomouc, Czech Republic

Pavel Bakala[c]
Institute of Physics, Faculty of Philosophy and Science, Silesian University in Opava, Bezručovo nám. 13, CZ-74601 Opava, Czech Republic

(Received 17 January 2016; accepted 19 October 2016)

Life is dependent on the income of energy with low entropy and the disposal of energy with high entropy. On Earth, the low-entropy energy is provided by solar radiation and the high-entropy energy is disposed of as infrared radiation emitted into cold space. Here, we turn the situation around and imagine the cosmic background radiation as the low-entropy source of energy for a planet orbiting a black hole into which the high-entropy energy is expelled. We estimate the power that can be produced by thermodynamic processes on such a planet, with a particular interest in planets orbiting a fast rotating Kerr black hole as in the science fiction movie *Interstellar*. We also briefly discuss a reverse Dyson sphere absorbing cosmic background radiation from the outside and dumping waste energy to a black hole inside.
[http://dx.doi.org/10.1119/1.4966905]

I. INTRODUCTION

Life on Earth is possible thanks to the hot Sun and the cold sky. Their temperature difference makes it possible to drive processes far from thermodynamic equilibrium by increasing the entropy elsewhere in the universe. Absorbing photons from the Sun at ∼6000 K and emitting about 20 times more photons at ∼300 K to the cold sky makes the entropy balance sufficient to sustain complex processes in which entropy locally drops. As explained by Erwin Schrödinger in his book *What is life?*,[1] organisms feed on negative entropy. The hot Sun and cold skies provide the Earth with a great deal of negative entropy; in this way, the Earth produces $\sim 5 \times 10^{14}$ J/K of entropy each second.[2]

Here, we play with the idea of a world upside down: the Sun is cold and skies are "hot." Let us imagine a planet orbiting a black hole in a universe filled with background radiation. The inhabitants accept low-entropy energy from the sky and expel waste heat to the black hole. The protagonists of the recent movie *Intersellar*, who want to colonize a planet orbiting a supermassive black hole *Gargantua*, might find these results vital (for physical details of their trip and destination, we recommend the book *The Science of Interstellar*[3] by Kip Thorne, the scientific consultant and an executive producer of the film).

Apart from the pedagogical value of simple thermodynamic exercises, these speculations might be relevant in the distant future when stars exhaust their nuclear fuel and die, and black holes may become dominant constituents of the entropy production processes.[4,5] This kind of energetics might be useful until the expansion of the universe cools the cosmic background radiation below the temperature of the black hole Hawking radiation. After that, the black hole becomes a net radiator and thus the nearby inhabitants might again live under a hot sun and cold sky. Recently, we discussed in this journal a mechanism of extracting mechanical work from radiating black holes;[6] however, the focus here is on the not-so-distant future.

The ideas presented here could also be relevant to the early stages of the universe. Recently, Loeb[7] suggested that a habitable epoch occurred when the universe was about 15×10^6 years old and the background radiation had a temperature of 273–300 K, allowing for rocky planets with liquid-water chemistry on their surfaces. This suggestion was covered by *Nature*,[8] mentioning also some criticism pointing out that the cold sky is thermodynamically as important for Earth's life as the hot Sun. The black-hole sun discussed here could be a source of the needed negative entropy in this early-universe scenario.

This paper is organized as follows. Section II presents general formulas for converting the incoming background radiation energy into useful work. Section III investigates two special regimes for the solid angle—large and small—of the incoming radiation. In Sec. IV, the results for anisotropic radiation due to high-speed orbiting close to the black hole are presented. Section V considers a Dyson sphere enclosing a black hole, and Sec. VI presents our conclusions. Details of the computations of the temperature map of the sky for an observer orbiting a black hole are given in the appendices.

II. RADIATION HEAT EXCHANGE

A. Sky projection and etendue conservation

Let us assume that radiative heat transfers to and from the planet can occur over a total surface area S. The celestial sphere[9] is divided into two parts: one is hot at temperature T_1 and the other cold, for simplicity at temperature absolute zero. Taking the black-hole temperature to be zero is a good approximation if Hawking radiation[10,11] is negligible. Let the solid angles spanned by these two parts of the celestial sphere be Ω_H and Ω_C, with $\Omega_H + \Omega_C = 4\pi$. To allow for the most efficient thermal energy exchange between the planet and the sky, we assume the entire planet to be covered with light concentration systems that project the celestial sphere into its images. We assume the numerical aperture of these devices approaches 1, which means that each point of the image is uniformly illuminated from the 2π solid angle by rays coming from the corresponding point of the object (see Fig. 1). This means that each part of the image can interact as a Lambertian radiator with the corresponding part of the sky (the defining feature of the Lambertian radiator is that its surface has the same radiance when viewed from any angle).

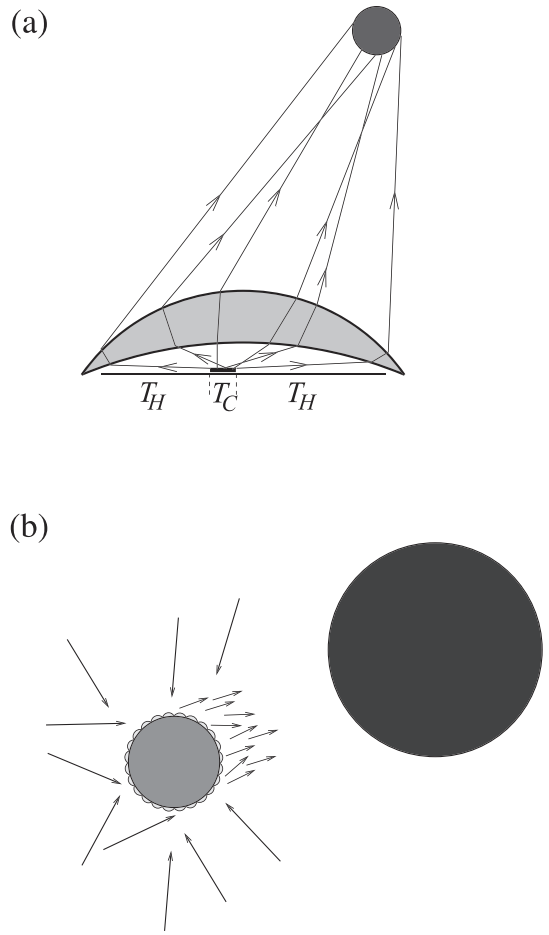

Fig. 1. (a) Projection system for interaction of a Lambertian radiator with the black hole. The arrows represent radiation from the cold surface at temperature T_c directed to the black hole. The remaining surface at temperature T_H interacts by radiation (not shown) with the hot sky. (b) Scheme of the thermodynamic system: the planet covered with the light concentration systems shown in (a) accepts high-energy photons (long arrows) from space and sends low-energy photons (short arrows) to the black hole.

In this way, all rays coming from the hot part of the sky are projected to one part of the surface of the planet and rays from the cold part to another. Let us denote the areas of these surfaces S_H and S_C with $S_H + S_C = S$.

For the bundle of all possible rays going through some area of the system, we can introduce a quantity called etendue (or étendue), which is equal to the area multiplied by the solid angle occupied by all the ray directions. Generally, etendue characterizes how the light is spread in area and angle, and, when multiplied by radiance, gives the radiation power. A general theorem of ray optics says that the etendue for propagating light cannot decrease (see, e.g., Ref. 12). For a part of a beam propagating in directions within a solid angle $\delta\Omega$ across a surface element δA, the element of etendue is defined as $\delta\mathcal{E} = n^2 \cos\theta\, \delta\Omega\, \delta A$, where n is the refraction index of the medium and θ is the angle between the direction of propagation and the normal to δA. If the light propagates through a non-absorbing, non-scattering environment (such as through our idealized optical systems), the etendue is conserved. This result is analogous to phase-space conservation in conservative mechanical systems according to the Liouville theorem. For our scheme, the consequence of etendue conservation is that

$$\frac{S_H}{S_C} = \frac{\Omega_H}{\Omega_C}. \tag{1}$$

This relationship tells us that the total surface of the planet can be divided into two parts S_H and S_C serving as the hot and cold terminals of heat engines, their proportion being equal to the proportion of the hot and cold parts of the sky.

Without the idealization leading to Eq. (1), one would have to take into account the fact that the cold terminal also interacts with objects at higher temperature, which would decrease the efficiency of work production. Let us note that in the photovoltaic industry one of the goals is the construction of light concentrators approaching the etendue limit (see, e.g., Ref. 13), so we assume that the advanced civilization inhabiting the planet under study has reached this goal.

B. Temperature optimization for given S_H and S_C

Let the surfaces of the heat exchangers S_H and S_C be at temperatures T_H and T_C and let them serve as heat exchangers for a heat engine. The task is to find T_H and T_C such that the power of the heat engine is maximized. The procedure is analogous to the power optimization of irreversible engines as first studied by Novikov[14] and later independently in this journal by Curzon and Ahlborn[15] (for more general considerations see, e.g., Ref. 16). Our case is different in the temperature dependence of the thermal energy exchange rate ($\propto T^4$), and also in our having fixed the ratio of the exchanger surfaces, S_H/S_C.

The thermal energy received by S_H from the hot part of the sky during a time interval Δt is $Q_1 = \sigma S_H (T_1^4 - T_H^4)\Delta t$ and the waste energy sent to the cold part of the sky is $Q_2 = \sigma S_C T_C^4 \Delta t$, where $\sigma \approx 5.68 \times 10^{-8}$ W m^{-2} K^{-4} is the Stefan–Boltzmann constant. The difference between Q_1 and Q_2 can be converted into work $W = Q_1 - Q_2$ provided that $Q_1/Q_2 = T_H/T_C$ (in the limiting, optimum case). A relation between T_H and T_C follows from this assumption,

$$T_C = \left[\frac{S_H}{S_C}\left(\frac{T_1^4}{T_H^4} - 1\right)\right]^{1/3} T_H, \tag{2}$$

and the average power $P = W/\Delta t$ can therefore be expressed as

$$P = \sigma S_H \left[T_1^4 - T_H^4 - \left(\frac{S_H}{S_C}\right)^{1/3}\left(\frac{T_1^4}{T_H^4} - 1\right)^{4/3} T_H^4\right]. \tag{3}$$

Assuming that S_H, S_C, and T_1 are fixed, we can find T_H such that the power of the engine is maximized. Setting the derivative equal to zero, $dP/dT_H = 0$, we find

$$T_H = u^{1/4} T_1, \tag{4}$$

$$T_C = \left(\frac{S_H}{S_C}\right)^{1/3} \frac{(1-u)^{1/3}}{u^{1/12}} T_1, \tag{5}$$

where u solves the equation

$$\frac{27}{q} u^4 - 18u^2 - 8u - 1 = 0, \tag{6}$$

in the interval $0 < u < 1$, and

$$q \equiv \frac{S_H}{S} = \frac{\Omega_H}{4\pi}, \tag{7}$$

is the hot fraction of the sky. The resulting power is then

$$P_{\max} = \eta q \sigma S T_1^4, \tag{8}$$

where $q\sigma S T_1^4$ is the total power of the incoming radiation, and

$$\eta \equiv 1 - u - \left(\frac{q}{1-q}\right)^{1/3} u \left(\frac{1-u}{u}\right)^{4/3} \tag{9}$$

is the efficiency with which the incoming radiation can be converted into useful work.

Even though Eq. (6) as a quartic equation has an explicit solution, we solve it numerically and the result is used to find the dependence of the working temperatures T_H and T_C, and of the efficiency η, on the hot-sky fraction q, as shown in Fig. 2.

III. SPECIAL OPERATING REGIMES

A. Small heating area

Assuming $S_H \ll S_C$, or $q \ll 1$, Eq. (6) yields $u \approx 3^{-3/4} q^{1/4}$ and the temperatures approach zero as

$$T_H \approx 3^{-3/16} q^{1/16} T_1, \tag{10}$$

$$T_C \approx 3^{1/16} q^{5/16} T_1 \tag{11}$$

(see Fig. 2), while the efficiency η of the process approaches 1 as

$$\eta \approx 1 - (3q)^{1/4}. \tag{12}$$

This limit corresponds not to a "standard" black hole, but rather to a distant star illuminating a planet in an otherwise empty universe. (The relevance to a less conventional black hole situation will be discussed later in Sec. IV B.) The results can be applied to estimate Earth's energy income from our Sun. In this case, $q \approx 5.4 \times 10^{-6}$ and $T_1 = 5778\,\mathrm{K}$, which leads to working temperatures $T_H = 0.385\ T_1 \approx 2200\,\mathrm{K}$ and $T_C = 0.0239\ T_1 \approx 138\,\mathrm{K}$. The efficiency is then 92% and the maximum available power is $P \approx 1.603 \times 10^{17}\,\mathrm{W}$. This is 4 orders of magnitude above what our present-day society uses.

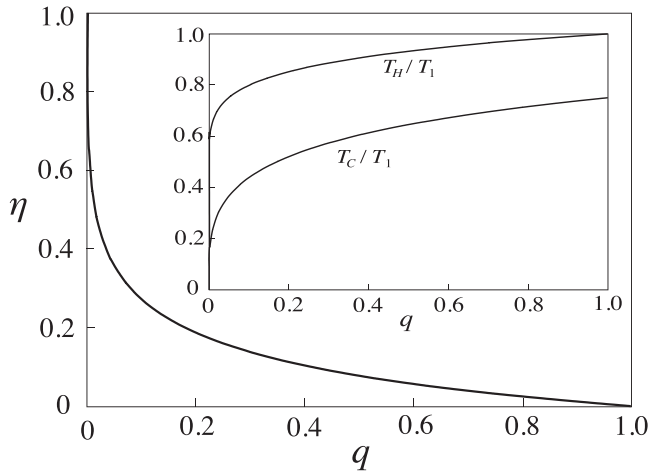

Fig. 2. Efficiency η as a function of the hot area fraction q for optimized power, according to Eq. (9). Inset: temperatures of the hot and cold surfaces as functions of q.

B. Large heating area

In the opposite limit $S_H \to S$, and on solving Eq. (6) for $1 - q \ll 1$, we find

$$u \approx 1 - \frac{3^3}{2^6}(1-q), \tag{13}$$

which leads to

$$T_H \approx \left[1 - \frac{3^3}{2^8}(1-q)\right] T_1, \tag{14}$$

$$T_C \approx \frac{3}{4}\left[1 - \frac{3^4}{2^8}(1-q)\right] T_1, \tag{15}$$

$$\eta \approx \frac{3^3}{2^8}(1-q). \tag{16}$$

Using these expressions in Eq. (8), we find the power of maximum work generation

$$P_{\max} \approx \frac{3^3}{2^8} \sigma S_C T_1^4. \tag{17}$$

As an illustration, let us assume a planet of Earth's size orbiting a black hole whose angular size as seen from the planet is equal to the angular size of Sun as seen from Earth. This leads to $q \approx 1 - 5.4 \times 10^{-6}$ and $\eta \approx 5.7 \times 10^{-7}$. Thus, $S_C \approx 2760\,\mathrm{km}^2$, so that the planet would radiate its waste thermal energy from an area comparable to Rhode Island. If the background radiation is at room temperature $T_1 = 300\,\mathrm{K}$ as in the 15×10^6-year-old universe assumed in Ref. 7, then $T_C \approx 225\,\mathrm{K}$, i.e., about –48 °C. From Eq. (17), we find that useful work could then be obtained with power $P_{\max} \approx 130\,\mathrm{GW}$. This is 2 orders of magnitude below the present world energy consumption, and 6 orders of magnitude below the power presently supplied to Earth by our Sun. The background radiation of today's skies is 2 orders of magnitude colder at $T_1 = 2.725\,\mathrm{K}$, which results in even less available useful power: $P \approx 910\,\mathrm{W}$.

IV. CIRCULAR MOTION CLOSE TO THE BLACK HOLE

Because η increases with decreasing q, to get as much power as possible we should place the orbit as close to the black hole as possible. However, things get complicated there: the observer moves fast and relativistic effects become important. The absorbed radiation is Doppler-shifted, as well as blue-shifted by falling to the vicinity of the black hole. The influence of the gravitational blue-shift on the cosmic background radiation for an observer close to the event horizon of the Schwarzschild (i.e., nonrotating) black hole was recently studied in Ref. 17. Here, we consider an observer located on the planet orbiting the black hole, both Schwarzschild and Kerr (i.e., rotating). As a result of the motion, the sky ceases to be isothermal—the radiation comes hotter from the direction in front of the observer and colder from the rear. To get an accurate picture of the sky, computations outlined in Appendices A and B have been carried out; the results are

shown in Figs. 3 and 4. Having the temperature map of the sky, one can use segments of the sky with different temperatures as heaters and apply another optimization to allocate to them various parts of the cooling area so as to get maximum power.

A. Schwarzschild black hole

We first consider motion along a timelike circular geodesic around a static, spherically symmetric black hole of mass M and Schwarzschild radius $R_S = 2GM/c^2$, where G is the gravitational constant and c is the speed of light. Stable bound circular orbits of radius r exist for $r \geq 3R_S = 6GM/c^2$ (see, e.g., Refs. 18 and 19). In order to obtain the maximum power, the innermost stable circular orbit at $r = 6GM/c^2$ has been chosen. The resulting picture of the sky is shown in Fig. 3(a). The shadow of the black hole covers 12.2% of the sky, i.e., $q = 0.878$. If the temperature shifts were disregarded,

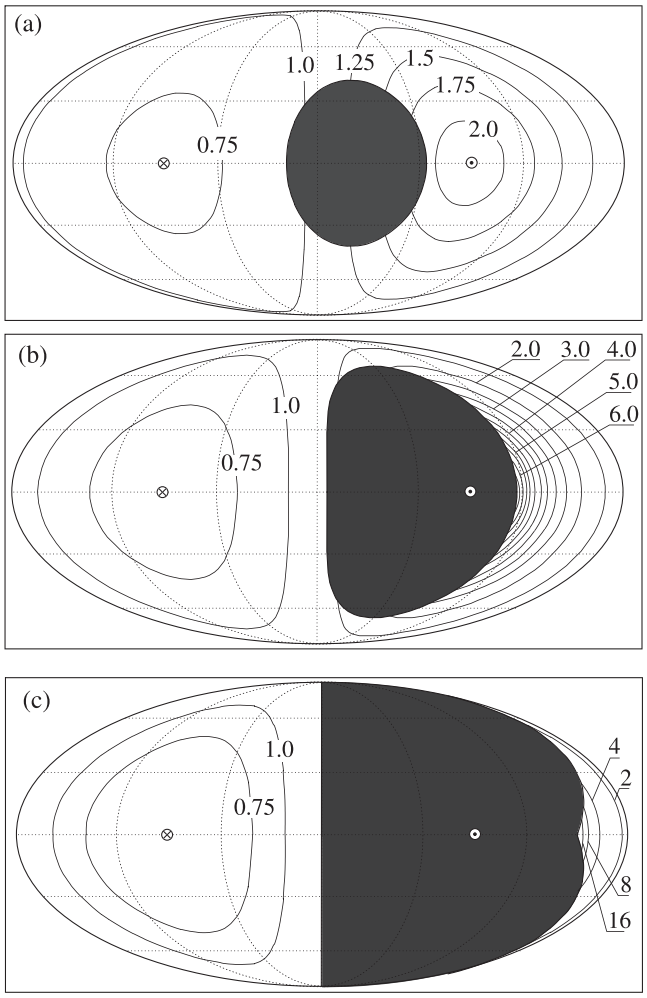

Fig. 3. Mollweide projection of the sky of an observer orbiting a black hole. The dark area is the shadow of the black hole, while the solid lines are contour lines of constant temperature, where the numbers indicate relative temperature shifts with respect to the temperature of the background radiation as measured by a distant observer. The symbols ⊙ and ⊗ indicate the directions to which and from which the observer is moving, respectively. The dotted lines are parallels of latitude at $\theta = 0, \pm 30°$, and $\pm 60°$, and meridians of longitude at $\phi = 0, \pm 60°$, and $\pm 120°$. (a) A nonrotating black hole with the orbit at $r = 6GM/c^2$; (b) a rotating black hole with rotation parameter $a = 1 - 1.3 \times 10^{-14}$ and orbit radius $r = 2.2GM/c^2$; (c) a rotating black hole with $a = 1 - 1.3 \times 10^{-14}$ and $r = 1.0000379GM/c^2$.

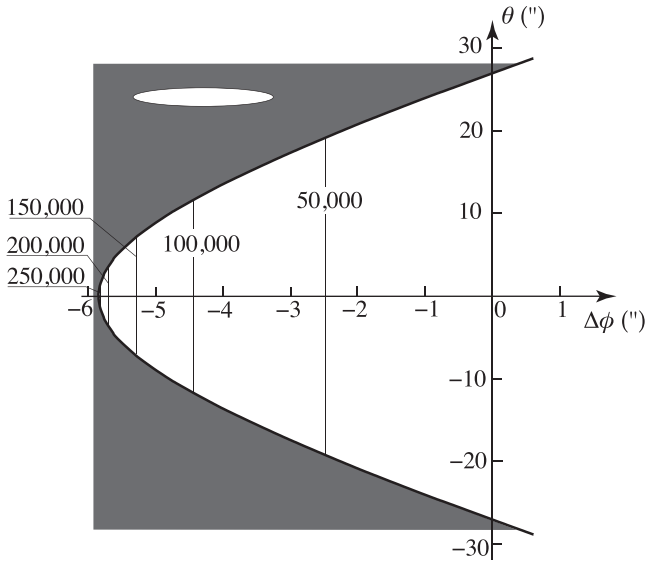

Fig. 4. Details of the shadow boundary of a black hole for the case of Fig. 3(c) near $\theta = 0$ and $\phi = 150°$, where $\Delta\phi \equiv \phi - 150°$. The contour lines of constant temperature are shown, the numbers indicating relative temperature shifts with respect to the temperature of the background radiation as measured by a distant observer. The light spot at the upper left shows the angular size of Neptune as seen from the Earth, for comparison (the shape is deformed due to different scales of θ and $\Delta\phi$).

Eqs. (6), (8), and (9) would yield $\eta \approx 1.39\%$ and $P_{\max} \approx 0.012\sigma S T_1^4$. For an Earth-sized planet and background radiation at $T_1 = 2.725$ K, this would be $P_{\max} \approx 19$ MW.

However, fast motion around the black hole makes parts of the sky warmer, which brings some advantages. As seen in Fig. 3(a), the sky temperature is more than twice as large measured by the orbiting observer in the direction of motion compared to an observer at rest and far from the black hole (the maximum blue shift being $3/\sqrt{2} \approx 2.12$; see Appendix A for the derivation). Thus, the power available from this part of the sky can be more than 2^4 times larger than without the blue shift. However, the hottest part of the sky is relatively small and the rest of the sky is colder. To find the total available power, we have divided the hot sky into 30 segments of equal temperature-span intervals. Each segment then serves as the heater of a separate heat engine. Since the power of each engine also depends on the cold area used for dumping its waste energy, one has to find the optimum allocation of the cold area to the individual engines to obtain a maximum total power. The result of the numerical optimization is shown in Fig. 5(a). The white bars are the areas of the hot segments, which are given as the input data. The black bars are the areas of the corresponding cold segments obtained as the result of the optimization procedure. As can be seen, the optimum allocation assumes absorbing radiation from the 14 hottest segments of blueshifts above 1.4. Colder parts of the hot sky are not worth using as hot reservoirs. The resulting power is then $P_{\max} \approx 0.126\sigma S T_1^4$, 1 order of magnitude larger than the above estimate based on disregarding the frequency shifts. For an Earth-sized planet and background radiation at $T_1 = 2.725$ K, this would be $P_{\max} \approx 200$ MW, still rather low for a comfortable life of more than a few small towns.

B. Fast rotating Kerr black hole

How can we come closer to the black hole so as to increase the cold sky proportion? We were inspired by the

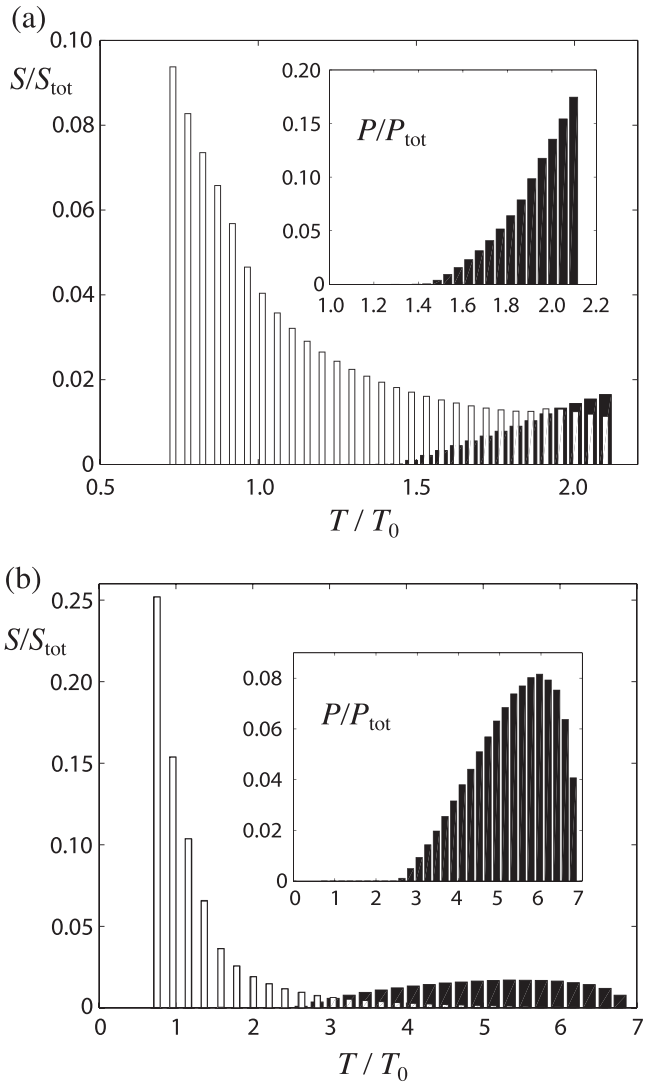

Fig. 5. Empty bars: fractions of the observer's sky at different temperatures, where the hot sky is divided into 30 segments of equal temperature span. Full bars: fractions of the observer's sky used as cold reservoirs for heat engines of upper temperature T. All bars sum up to 1, the empty bars sum up to the fraction of the radiating sky, and the full bars sum up to the fraction covered by the shadow of black hole. Inset: fractions of the power of the heat engines with upper temperature T; the bars sum up to 1. (a) Schwarzschild black hole with orbit at $r = 6GM/c^2$ as in Fig. 3(a); (b) Kerr black hole with $a = 1 - 1.3 \times 10^{-14}$ and orbit at $r = 2.2GM/c^2$ as in Fig. 3(b).

movie *Interstellar*, where the characters come close to a fast-rotating giant black hole named *Gargantua*. Rotating black holes give rise to stable circular orbits closer than $6GM/c^2$. For Gargantua, the rotation parameter a was extraordinarily large, $a = 1\text{–}1.3 \times 10^{-14}$, thus allowing the characters to enjoy extraordinarily strong relativistic effects close to the black hole.[3,20] We have computed the results for two special cases of the orbit radius, $r = 2.2GM/c^2$ [Figs. 3(b) and 5(b)] and $r = 1.0000379GM/c^2$ [Figs. 3(c) and 4]. The latter case corresponds to the orbit of *Miller's planet*, where the characters of Interstellar spend 3 h while 21 years pass on their base station, far from the reach of Gargantua's gravitational time shift.

We can see in both cases that the shadow of the black hole becomes deformed and covers a large part of the observer's sky, including the direction toward which the planet is moving. Nevertheless, the planet does not fall into the hole as it is dragged by the rotating gravitational field. The blue shift becomes much stronger, although in relatively small strips of the sky just above the shadow of the black hole in the direction of the planet's motion. In the case $r = 2.2GM/c^2$ the black hole covers 26% of the sky and the maximum blue shift is 6.90. Upon using the same optimization procedure as in Subsec. IV A, one finds the maximum attainable power to be $P_{\rm max} \approx 4.2\sigma S T_1^4$. For an Earth-sized planet and background radiation at $T_1 = 2.725\,\text{K}$ this would be $P_{\rm max} \approx 6.7\,\text{GW}$, i.e., enough for a small country.

The case of Miller's planet with $r = 1.0000379GM/c^2$ leads to extreme blue shifts, reaching up to 275 000. The black hole covers 40% of the sky and most of the radiation energy comes from a very narrow strip of a few arcseconds (see Fig. 4); our numerical results show that 99% of the energy comes from a strip of longitude span 2.3 in. and latitude span 5.8 in. This size is comparable, e.g., to the angular size of the planet Neptune as seen from Earth, with angular diameter ≈2.2 in. Thus, the good news is that Miller's planet enjoys a small-heating-area regime (see Sec. III A), meaning that most of the incoming radiation energy can be converted into useful work. The bad news for the visiting astronauts is that it is too much energy: the incoming flux density (power per unit area perpendicular to the incoming radiation) is $\Phi \approx 420\,\text{kW/m}^2$, i.e., about 300 times larger than the solar constant. This value can be used to find the equilibrium temperature of a planet radiating its energy as a black body, resulting in $T = \sqrt[4]{\Phi/(4\sigma)} \approx 890\,^\circ\text{C}$. Thus, the tidal waves observed on the planet might be, e.g., of melted aluminum. Moreover, the astronauts would be grilled by extreme-UV radiation.

V. BLACK HOLE DYSON SPHERE

Rather than assuming a planet, one could imagine a spherical shell enclosing the black hole. In 1960, Freeman Dyson speculated about possible signatures of intelligent extraterrestrial life that would build a structure around a star to capture all of its power.[21] The waste thermal energy would be emitted as infrared radiation detectable by our observatories. We can turn this idea upside down: the inhabitants of the shell collect energy from the background radiation and send the waste thermal energy to the central black hole (see Fig. 6).

To explore the properties of such a scheme, we can use the results of Sec. II B. However, we assume that the total area is not fixed, but variable—determined by the radius of the Dyson sphere R_D. The sphere collects thermal energy from the outer area $S_H = 4\pi R_D^2$. With respect to the cold area, the situation is now simpler than in Sec. II A because no light concentrators are necessary. The waste energy is radiated from the entire inner surface and the emitted photon either hits the black hole or is absorbed by another part of the inner surface. Thus, the waste energy is absorbed by the shadow of the black hole, which for a distant observer looks like a sphere of radius $(\sqrt{27}/2)R_S$ (see Ref. 22), and therefore, $S_C = 108\pi G^2 M^2/c^4$.

The available power increases as we increase the Dyson sphere radius, up to a limit given by the fixed area of the heat sink. To calculate the limiting power, we assume $R_D \gg R_S$ and apply the results of Sec. III B with $S_C/S_H \ll 1$. In this case, the limiting power follows from Eq. (17) as $P_{\rm max} \approx 0.1055 P_{\rm ref}$, where $P_{\rm ref} = \sigma S_C T_1^4$ is the power of the background radiation that would be absorbed by the black hole if there were no Dyson sphere.

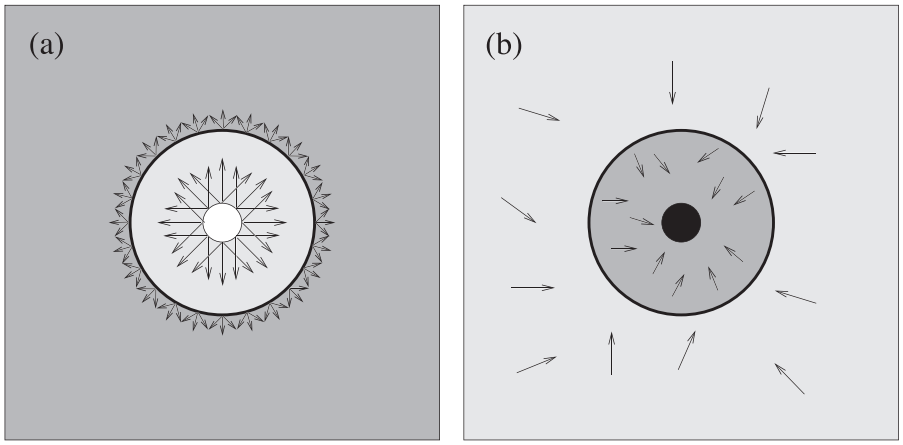

Fig. 6. Scheme of the Dyson sphere (a) and of its black-hole version (b). In the original version (Ref. 21) the shell captures radiation emitted by the star inside and radiates waste heat out to space. In the black-hole version, the shell absorbs background radiation coming from outside and emits waste heat to the black hole inside.

As an illustration, we first consider a black hole with the mass of our Sun, $M = 2 \times 10^{30}$ kg, and use the present temperature of the background radiation, $T_1 = 2.725$ K; then the limiting power is $P_{\max} \approx 250$ W. On the other hand, a supermassive black hole of $\sim 4 \times 10^6$ solar masses (e.g., the one in the center of our galaxy) could give $P_{\max} \sim 4 \times 10^{15}$ W, about 200 times our present world energy consumption (ignoring, however, the solar power harvested by the ecosystems). As a last example, we consider the early universe background radiation with $T_1 \approx 300$ K and a black hole with apparent radius equal to the radius of our Sun, i.e., $(\sqrt{27}/2)R_S \approx 6.96 \times 10^8$ m. This scenario gives $P_{\max} \approx 2.9 \times 10^{20}$ W, which is 3 orders of magnitude above the present solar energy income of Earth.

VI. CONCLUSION

For nonrotating black holes and the present temperature of the cosmic microwave background, the available power appears to be rather small for the living standards of our civilization. One might speculate of the distant future when hydrogen as the nuclear fuel for stars is exhausted and black holes together with background radiation become one of the few relevant sources of negative entropy. However, with the accelerated expansion of the universe the background radiation becomes colder so that even less power would be available. One might also speculate about hypothetical Earth-like planets orbiting primordial black holes in the early stages of the universe filled with room-temperature background radiation. The available power budget is much more generous in this scenario, but one could hardly expect that organisms with the necessary radiation-focusing equipment would stand a chance to evolve.

The situation is different for fast-rotating Kerr black holes and planets in close orbits; gravitational and Doppler shifts change the temperature map of the sky to allow for harvesting much more power. Although the idea of exploring planets orbiting Kerr black holes, as depicted in *Interstellar*, is appealing, the conditions on Miller's planet of the film prove to be rather harsh. This could be expected: since the time dilation on the planet is about 60 000, the astronauts would receive signals from the distant outside arriving about 60 000 times faster than emitted. Such a frequency shift must apply also to the cosmic background, making it much hotter. Nevertheless, with a suitably chosen orbit slightly farther from Gargantua, one could hope to find a planet with sky conditions much closer to terrestrial.

APPENDIX A: FREQUENCY SHIFT AND TEMPERATURE MAP OF THE SKY FOR AN OBSERVER ORBITING A SCHWARZSCHILD BLACK HOLE

Here, we derive the angular dependence of the frequency shift for an observer in a circular orbit around a Schwarzschild black hole. The frequency ratio between the locally observed and emitted frequencies of ray bundles $g = \nu_{\text{obs}}/\nu_\infty = p^{\langle t \rangle}/p_t$ also corresponds to the ratio of the locally measured and emitted energies (time components of photon four-momentum). Here and hereafter, the angle brackets in the index denote the local frame of the observer on the Keplerian orbit. The source intensity divided by the third power of the frequency is conserved as a Lorentz invariant.[23] Moreover, Planck's law gives the spectral intensity of blackbody radiation, proportional to $\nu^3/(e^{h\nu/kT} - 1)$, where T is the source temperature, ν is the frequency, h is Planck's constant, and k is Boltzmann's constant. Therefore, the blackbody spectrum of the background radiation will be locally observed as a blackbody spectrum with a temperature multiplied by the factor g related to a particular ray bundle. Naturally, the bolometric intensity amplification of ray bundles coming from the distant universe is given by the fourth power of g. Here, as usual, the bolometric intensity corresponds to the total flux of radiation at all wavelengths per the solid angle (in W m^{-2} sr^{-1}).

Using the $(-+++)$ metric signature, geometrical units $(c = G = 1)$, and common Schwarzschild coordinates $(t, r, \vartheta, \varphi)$, the spacetime metric can be expressed in the well-known form

$$ds^2 = -\left(1 - \frac{2M}{r}\right) dt^2 + \frac{dr^2}{1 - 2M/r} + r^2\left(d\vartheta^2 + \sin^2\vartheta\, d\varphi^2\right). \tag{A1}$$

As derived in various textbooks (see, e.g., Ref. 19, p. 200 or Ref. 18, p. 29), the four-velocity of an observer in the equatorial plane $\vartheta = \pi/2$ with constant r has two nonzero components

$$u^t_{\rm obs} = \frac{dt}{d\tau}, \tag{A2}$$

$$u^\varphi_{\rm obs} = \frac{d\varphi}{d\tau} = \frac{d\varphi}{dt}\frac{dt}{d\tau} = u^t_{\rm obs}\frac{d\varphi}{dt}, \tag{A3}$$

where τ is the observer's proper time. Moreover, the circular trajectories obey Kepler's law (again, see, e.g., Refs. 18 and 19)

$$\Omega = \frac{d\varphi}{dt} = \sqrt{\frac{M}{r^3}}. \tag{A4}$$

The normalization condition $\mathbf{u}_{\rm obs}\cdot\mathbf{u}_{\rm obs} = -1$ then leads to

$$\frac{dt}{d\tau} = \frac{1}{\sqrt{1-3M/r}}, \tag{A5}$$

and, consequently,

$$u^t_{\rm obs} = \frac{1}{\sqrt{1-3M/r}}, \quad u^\varphi_{\rm obs} = \sqrt{\frac{M/r^3}{1-3M/r}}. \tag{A6}$$

Analogously,[18,19] for a stationary observer hovering at the same constant r the only nonzero four-velocity component is

$$u^t_{\rm stat} = \frac{1}{\sqrt{1-2M/r}}. \tag{A7}$$

The orbital speed v of an orbiting observer with respect the stationary one at the same r is determined by the Lorentz factor $\gamma = (1-v^2)^{-1/2}$

$$\gamma = -\mathbf{u}_{\rm obs}\cdot\mathbf{u}_{\rm stat} = -g_{tt}u^t_{\rm obs}u^t_{\rm stat} = \sqrt{\frac{1-2M/r}{1-3M/r}}, \tag{A8}$$

$$v = \sqrt{\frac{M/r}{1-2M/r}}. \tag{A9}$$

For an observer following the innermost stable circular orbit at $r = 6M$ we get $v = 1/2$.

The frequency shift of a photon coming from infinity includes an r-dependent gravitational blue-shift (that would also be detected by a stationary observer) and a kinematic Doppler shift determined by the orbital velocity v and the direction of light propagation. The gravitational blue-shift is described by the well-known formula[18,19]

$$\nu_{\rm stat} = \frac{\nu_\infty}{\sqrt{1-2M/r}}, \tag{A10}$$

where ν_∞ is the photon frequency at infinity and $\nu_{\rm stat}$ is the frequency detected by the stationary observer at r. From the Doppler-shift formula,[18,19] we obtain

$$\nu_{\rm stat} = \gamma\nu_{\rm obs}(1 + v\cos\alpha'), \tag{A11}$$

where α' is an angle between the observer's velocity and the direction of light propagation measured in the observer's frame of reference. Combining Eqs. (A10) and (A11), we come to the final formula for the frequency shift detected by an orbiting observer

$$g = \frac{\nu_{\rm obs}}{\nu_\infty} = \frac{\sqrt{1-3M/r}}{1-2M/r}\left(1 + \sqrt{\frac{M/r}{1-2M/r}}\cos\alpha'\right)^{-1}. \tag{A12}$$

The case of the innermost stable trajectory with $r = 6M$ is shown in Fig. 3(a). Using $r = 6M$ and $\cos\alpha' = \mp 1$ in Eq. (A12), we obtain $g_- = 3/\sqrt{2} \approx 2.12$ for photons striking the observer at the innermost stable trajectory from ahead (the value mentioned in Sec. IV A), and $g_+ = 1/\sqrt{2} \approx 0.71$ for photons arriving at the same observer from the rear.

Alternatively, the result can be derived from the photon four-momentum $\mathbf{p}_{\rm ph}$. The photon energy detected by an observer with four-velocity $\mathbf{u}_{\rm obs}$ is[19]

$$E_{\rm obs} = h\nu_{\rm obs} = -\mathbf{p}_{\rm ph}\cdot\mathbf{u}_{\rm obs}. \tag{A13}$$

Because of the symmetries of the Schwarzschild metric, two quantities are conserved along light ray orbits in the equatorial plane, namely,

$$p_\varphi = L_{\rm ph} = r^2 p^\varphi_{\rm ph}, \tag{A14}$$

$$p_t = E_{\rm ph} = h\nu_\infty = \left(1 - \frac{2M}{r}\right)p^t_{\rm ph}. \tag{A15}$$

These quantities are connected with the photon's angular momentum $L_{\rm ph}$ and energy $E_{\rm ph}$ at infinity. From the normalization condition $\mathbf{p}_{\rm ph}\cdot\mathbf{p}_{\rm ph} = 0$ it follows that

$$p^t_{\rm ph} = \frac{h\nu_\infty}{1-2M/r}, \; p^\varphi_{\rm ph} = \frac{h\nu_\infty}{r\sqrt{1-2M/r}}. \tag{A16}$$

For the photon in the equatorial plane these are the only nonzero four-momentum components. Because of the spacetime symmetry, for a photon coming at an angle α seen by the stationary observer at constant r, substituting from Eqs. (A16) and (A6) into Eq. (A13) the photon momentum can be written in the form

$$h\nu_{\rm obs} = -g_{tt}p^t_{\rm ph}u^t_{\rm obs} - g_{\varphi\varphi}p^\varphi_{\rm ph}u^\varphi_{\rm obs}\cos\alpha. \tag{A17}$$

One can express this result by means of α' measured by the orbiting observer on applying the relativistic aberration formula (see, e.g., Ref. 19, p. 93)

$$\cos\alpha = \frac{\cos\alpha' + v}{1 + v\cos\alpha'}. \tag{A18}$$

After some algebraic manipulation we again come to Eq. (A12).

APPENDIX B: FREQUENCY SHIFT FOR AN OBSERVER ORBITING A KERR BLACK HOLE

The relativistic frequency-ratio factor g for an observer orbiting a Kerr black hole is obtained by following the same logic as in Appendix A, but we find it numerically by computing multiple relativistic projections of ray bundles on the observer's celestial sphere.[24,25] The line element of the Kerr spacetime in Boyer–Lindquist coordinates parameterized by specific angular momentum (spin) a reads

$$ds^2 = -\left(1 - \frac{2r}{\Sigma}\right) dt^2 - \frac{4ra}{\Sigma} \sin^2\theta \, dt \, d\varphi + \frac{\Sigma}{\Delta} dr^2 + \Sigma \, d\theta^2 + \left(r^2 + a^2 + \frac{2ra^2 \sin^2\theta}{\Sigma}\right) \sin^2\theta \, d\varphi^2, \tag{B1}$$

where $\Sigma \equiv r^2 + a^2 \cos^2\theta$ and $\Delta \equiv r^2 - 2r + a^2$. Components of the four-momentum of a photon in the Kerr spacetime are given by

$$\begin{aligned} p^r &= \dot{r} = s_r \Sigma^{-1} \sqrt{R_{\lambda,q}(r)}, \\ p^\theta &= \dot{\theta} = s_\theta \Sigma^{-1} \sqrt{\Theta_{\lambda,q}(\theta)}, \\ p^\phi &= \dot{\phi} = \Sigma^{-1}\Delta^{-1}[2ar + \lambda(\Sigma^2 - 2r)\mathrm{cosec}^2\theta], \\ p^t &= \dot{t} = \Sigma^{-1}\Delta^{-1}(\Sigma^2 - 2ar\lambda), \end{aligned} \tag{B2}$$

where the dotted quantities denote differentiation with respect to some affine parameter, and the sign pair s_r, s_θ describes the orientation of radial and latitudinal evolution, respectively.[26–28] The radial and latitudinal effective potentials read as

$$\begin{aligned} R_{\lambda,q}(r) &= (r^2 + a^2 - a\lambda)^2 - \Delta[q + (\lambda - a)^2], \\ \Theta_{\lambda,q}(\theta) &= q + a^2 \cos^2\theta - \lambda^2 \mathrm{cot}^2\theta. \end{aligned} \tag{B3}$$

Here, λ and q are constants of motion related to the covariant components of the photon four-momentum (B6) by the relations

$$\begin{aligned} \lambda &= -\frac{p_\phi}{p_t}, \\ q &= \left(\frac{p_\theta}{p_t}\right)^2 + [\lambda \tan(\pi/2 - \theta)]^2 - a^2 \cos^2\theta. \end{aligned} \tag{B4}$$

In the local reference frame related to an arbitrary observer, the azimuthal and latitudinal components $p_{\langle\varphi\rangle}$, $p_{\langle\theta\rangle}$ of the photon four-momentum fully determine a projection of the corresponding ray onto the local sky. Assuming the photon energy is normalized to 1, the remaining components of $p_{\langle\mu\rangle}$ can be written as

$$p_{\langle t\rangle} = -1, \quad p_{\langle r\rangle} = \sqrt{1 - p_{\langle\theta\rangle}^2 - p_{\langle\varphi\rangle}^2}\,. \tag{B5}$$

One can obtain the coordinate covariant components of the four-momentum and related constants of motion (B4) by transforming the local components of $p_{\langle\mu\rangle}$, using appropriate frame tetrads of one-forms by the relation

$$p_\mu = \omega_\mu^{\langle\alpha\rangle} p_{\langle\alpha\rangle}. \tag{B6}$$

Then the frequency-ratio factor $g(\lambda, q)$ can be expressed as a function of constants of motion corresponding to the projection position on the observer's sky as

$$g(\lambda, q) = -\frac{1}{p_t(\lambda, q)}. \tag{B7}$$

The local tetrad of one-forms related to the observer on the corotating Keplerian orbit around a Kerr black hole can be obtained by the Lorentz boost of the ZAMO (zero angular momentum observers, locally non-rotating observers)[28,29] tetrad, which in the equatorial plane ($\theta = \pi/2$) takes the form[30]

$$\begin{aligned} \omega^{(t)} &= \left\{\sqrt{\frac{\Delta\Sigma}{A}}, 0, 0, 0\right\}, \\ \omega^{(r)} &= \left\{0, \sqrt{\Sigma/\Delta}, 0, 0\right\}, \\ \omega^{(\theta)} &= \left\{0, 0, \sqrt{\Sigma}, 0\right\}, \\ \omega^{(\varphi)} &= \left\{-\frac{2ar}{\sqrt{A\Sigma}}, 0, 0, \sqrt{\frac{A}{\Sigma}}\right\}, \end{aligned} \tag{B8}$$

where $A \equiv (r^2 + a^2)^2 - a^2\Delta$. The velocity β of corotating Keplerian observers with respect to the equatorial ZAMO frame can be written as[30]

$$\beta = \frac{r^2 + a^2 - 2a\sqrt{r}}{\sqrt{\Delta}(r^{3/2} + a)}. \tag{B9}$$

The tetrad (B8) straightforwardly transformed into the frame of corotating Keplerian observer reads

$$\begin{aligned} \omega^{\langle t\rangle} &= \gamma\left\{\omega_t^{(t)} - \beta\omega_t^{(\varphi)}, 0, 0, -\beta\omega_\varphi^{(\varphi)}\right\}, \\ \omega^{\langle r\rangle} &= \omega^{(r)}, \quad \omega^{\langle\theta\rangle} = \omega^{(\theta)}, \\ \omega^{\langle\varphi\rangle} &= \gamma\left\{\omega_t^{(\varphi)} - \beta\omega_t^{(t)}, 0, 0, \omega_\varphi^{(\varphi)}\right\}, \end{aligned} \tag{B10}$$

where $\gamma \equiv (1 - \beta^2)^{-1/2}$.

For such an observer located in the close vicinity of the event horizon, the factor g varies depending on the angular coordinates in the local sky as a result of the interplay between extreme gravitational lensing and optical effects of special relativity caused by the orbital motion of the Keplerian frame. In principle, applying the relations discussed above it is possible to construct the so-called critical loci curve, which forms a boundary between a projection of a distant universe and a shadow of the black hole in the local sky.[31,32] To avoid significant analytical difficulties associated with such an approach, we used our relativistic ray-tracing code LSDplus, which performs a time-reverse direct numerical integration of Eq. (B2).[25,33]

The projection of the black hole shadow on the local celestial sphere corresponds to rays coming to the observer from very close to the event horizon. The most blue-shifted rays coming from the distant universe are projected near the right side of the shadow edge and around the celestial equator (see Fig. 3). The shadow edge corresponds to rays tightly passing or just leaving the boundary of the black hole photosphere.[34] Therefore, the ray-tracing code must integrate photon trajectories as accurately as possible in order to precisely distinguish between the extremely blue-shifted rays coming from infinity and the rays leaving the photosphere. The Runge–Kutta method of the eighth-order (Dorman–Prince method)[35] used here integrates the null geodesics with the very satisfactory relative accuracy of 10^{-15}, which, in the case of a central black hole with stellar mass, corresponds to an accuracy on the order of 10^{-11} m in the radial coordinate.[25] Moreover, the code LSDplus allows one to focus on an arbitrarily chosen and arbitrarily sized rectangular part of

the local sky in the Mollweide projection (see Fig. 4) with resolution limited only by computer memory. We have used the screen resolution of 4000×2000 pixels.

The techniques described above allow one to trace the location of the shadow edge with a high precision (see Figs. 3 and 4). The relativistic frequency-ratio factor g given by Eq. (B7) for ray bundles coming from the distant universe is calculated by the code as well.

[a]Electronic mail: tomas.opatrny@upol.cz
[b]Electronic mail: lukas.richterek@upol.cz
[c]Electronic mail: pavel.bakala@fpf.slu.cz

[1]E. Schrödinger, *What is Life? The Physical Aspect of the Living Cell* (Cambridge U.P., Cambridge, 1944).
[2]The energy input/output of Earth is the solar constant $\sim$1.36 kW/m^2 multiplied by the disk area of Earth $\pi R^2 \approx 1.28 \times 10^{14}$ m^2, i.e., 1.74×10^{17} J each second; if this is divided by the temperature $\sim$300 K we obtain the estimate of the entropy production.
[3]K. S. Thorne, *The Science of Interstellar* (Norton, New York, 2014).
[4]S. Frautschi, "Entropy in an expanding universe," Science **217**(4560), 593–599 (1982).
[5]L. M. Krauss and G. D. Starkman, "Life, the universe, and nothing: Life and death in an ever-expanding universe," Astrophys. J. **531**(1), 22–30 (2000).
[6]T. Opatrný and L. Richterek, "Black hole heat engine," Am. J. Phys. **80**(1), 66–71 (2012).
[7]A. Loeb, "The habitable epoch of the early Universe," Int. J. Astrobiol. **13**(4), 337–339 (2014).
[8]Z. Merali, "Life possible in the early Universe," Nature **504**(7479), 201 (2013).
[9]The celestial sphere is an imaginary sphere of arbitrarily large radius concentric with the observer. It is a practical tool in spherical astronomy for projecting objects on the sky. In Fig. 3, we show the Mollweide projection of the celestial sphere with the light (dark) area representing its hot (cold) part, respectively. The Mollweide projection generally used for global maps of the world or night sky is an equal-area, pseudocylindrical map projection preserving the proportions of areas, which is important for our considerations. It represents the central meridian as a straight line segment with other meridians longer and bowed outward away from the central one. This projection maps the sphere into a proportional 2:1 ellipse (the length of the central meridian is a half of the equator length).
[10]S. W. Hawking, "Black holes and thermodynamics," Phys. Rev. D **13**(2), 191–197 (1976).
[11]S. W. Hawking, "The quantum mechanics of black holes," Sci. Am. **236**, 34–40 (1977).
[12]T. Markvart, "The thermodynamics of optical étendue," J. Opt. A: Pure Appl. Opt. **10**, 015008 (2008).
[13]R. Winston and J. M. Gordon, "Planar concentrators near the étendue limit," Opt. Lett. **30**(19), 2617–2619 (2005).
[14]I. I. Novikov, "The efficiency of atomic power stations (a review)," J. Nucl. Energy II **7**(1–2), 125–128 (1958) [translated from At. Energy 3, 409–412 (1957)].
[15]F. L. Curzon and B. Ahlborn, "Efficiency of a Carnot engine at maximum power output," Am. J. Phys. **43**(1), 22–24 (1975).
[16]A. Bejan, "Entropy generation minimization: The new thermodynamics of finite-size devices and finite-time processes," J. Appl. Phys. **79**(3), 1191–1218 (1996).
[17]M. Wielgus, G. F. R. Ellis, F. H. Vincent, and M. A. Abramowicz, "Cosmic background radiation in the vicinity of a Schwarzschild black hole: No classic firewall," Phys. Rev. D **90**(12), 124024 (2014).
[18]D. Raine and T. Edwin, *Black Holes: An Introduction* (Imperial College Press, London, 2009).
[19]J. B. Hartle, *Gravity: An Introduction to Einstein's General Relativity* (Addison Wesley, San Francisco, 2003).
[20]The rotation parameter a (spin) is defined as a specific intrinsic angular momentum of the Kerr black hole; see, e.g., Hartle, Ref. 19, Sec. 15.2. For $a = 0$ the Kerr solution becomes the Schwarzschild non-rotating spherically symmetric spacetime [see Eq. (B1)]. The maximum possible value $a = 1$ corresponds to an extreme Kerr black hole having a rotation velocity of the event horizon equal to the speed of light. The case $a > 1$ gives a hypothetical naked singularity.
[21]F. J. Dyson, "Search for artificial stellar sources of infrared radiation," Science **131**(3414), 1667–1668 (1960).
[22]As shown in Ref. 33, the apparent angular size of a Schwarzschild black hole for a distant stationary observer is $2\arccos\sqrt{1-(27/r^2)(1-2/r)}$, where r is the distance of the black hole center in units of GM/c^2. For $r \gg 1$ the angular size is the same as that of a sphere of radius $\sqrt{27}GM/c^2$ seen from the same distance.
[23]M. H. Johnson and E. Teller, "Intensity changes in the Doppler effect," Proc. Natl. Acad. Sci. U. S. A. **79**(4), 1340 (1982).
[24]O. James, E. von Tunzelmann, P. Franklin, and K. S. Thorne, "Gravitational lensing by spinning black holes in astrophysics, and in the movie Interstellar," Classical Quantum Gravity **32**(6), 065001 (2015).
[25]P. Bakala, K. Goluchová, G. Török, E. Šrámková, M. A. Abramowicz, F. H. Vincent, and G. P. Mazur, "Twin peak high-frequency quasi-periodic oscillations as a spectral imprint of dual oscillation modes of accretion tori," Astron. Astrophys. **581**, A35–A47 (2015).
[26]B. Carter, "Global structure of the Kerr family of gravitational fields," Phys. Rev. **174**(5), 1559–1571 (1968).
[27]S. Chandrasekhar, *The Mathematical Theory of Black Holes* (Clarendon Press, Oxford, 1983).
[28]C. W. Misner, K. S. Thorne, and J. A. Wheeler, *Gravitation* (Freeman, San Francisco, 1973).
[29]J. M. Bardeen, "A variational principle for rotating stars in general relativity," Astrophys. J. **162**, 71–95 (1970).
[30]J. Schee and Z. Stuchlík, "Optical phenomena in the field of Braneworld Kerr black holes," Int. J. Mod. Phys. D **18**(6), 983–1024 (2009).
[31]S. U. Viergutz, "Image generation in Kerr geometry. I. Analytical investigations on the stationary emitter-observer problem," Astron. Astrophys. **272**, 355–377 (1993).
[32]E. Teo, "Spherical photon orbits around a Kerr black hole," Gen. Relativ. Gravitation **35**(11), 1909–1926 (2003).
[33]P. Bakala, P. Čermák, S. Hledík, Z. Stuchlík, and K. Truparová, "Extreme gravitational lensing in vicinity of Schwarzschild-de Sitter black holes," Cent. Eur. J. Phys. **5**(4), 599–610 (2007).
[34]The photosphere of a Kerr black hole is a region of unstable spherical or circular photon orbits wrapping the black hole. The photosphere reaches its maximum extent in the equatorial plane between corotating and counter-rotating circular photon orbits, while it becomes infinitesimally thin on the polar axis (see Ref. 32).
[35]W. H. Press, S. A. Teukolsky, W. T. Vetterling, and B. P. Flannery, *Numerical Recipes in C++* (Cambridge U.P., New York, 2007).